Floquet state depletion in ac-driven circuit QED

Ming-Bo Chen, Bao-Chuan Wang, Sigmund Kohler, Yuan Kang, Ting Lin, Si-Si Gu, Hai-Ou Li, Guang-Can Guo, Xuedong Hu, Hong-Wen Jiang, Gang Cao, and Guo-Ping Guo

Phys. Rev. B **103**, 205428 — Published 28 May 2021

DOI: 10.1103/PhysRevB.103.205428

Floquet State Depletion in AC Driven Circuit QED

Ming-Bo Chen,[1,2,*] Bao-Chuan Wang,[1,2,*] Sigmund Kohler,[3,†] Yuan Kang,[1,2] Ting Lin,[1,2] Si-Si Gu,[1,2] Hai-Ou Li,[1,2] Guang-Can Guo,[1,2] Xuedong Hu,[4] Hong-Wen Jiang,[5] Gang Cao,[1,2,‡] and Guo-Ping Guo[1,2,6,§]

[1] *Key Lab of Quantum Information, CAS, University of Science and Technology of China, Hefei, China*
[2] *CAS Center for Excellence in Quantum Information and Quantum Physics, University of Science and Technology of China, Hefei, Anhui 230026, China*
[3] *Instituto de Ciencia de Materiales de Madrid, CSIC, E-28049 Madrid, Spain*
[4] *Department of Physics, University at Buffalo, SUNY, Buffalo, New York 14260-1500, USA*
[5] *Department of Physics and Astronomy, University of California at Los Angeles, California 90095, USA*
[6] *Origin Quantum Computing Company Limited, Hefei, Anhui 230026, China*

(Dated: April 27, 2021)

We perform Floquet spectroscopy in a GaAs double quantum dot system coupled to a high-impedance superconducting resonator. By applying microwave induced consecutive passages under a double resonance condition, we observe novel Landau-Zener-Stückelberg-Majorana interference patterns that stem from a cavity-assisted interference pattern modified by the depletion of the ground state. Our experimental results reveal the stationary state behavior of a strongly driven two-level system, and are consistent with the simulations based on our theoretical model. This study provides an excellent platform for investigating the dynamics of Floquet states in the presence of strong driving.

Driving a quantum two-level system strongly and periodically leads to a variety of quantum effects, such as Landau-Zener-Stückelberg-Majorana (LZSM) interference and multi-photon resonance [1, 2]. These phenomena provide clear evidence for the quantum coherence of a physical system [3–13] and can be employed to probe the energy spectrum [14, 15] and the Floquet spectrum [16]. Since driving and active gating are integral parts of the quantum circuit paradigm for quantum computing, a thorough understanding of the strongly driven dynamics of a qubit could help to explore the limits to qubit control and manipulation.

Theoretical investigations of driven dissipative systems yielded interesting results in recent years. For example, it has been shown that at low temperatures, the stationary state of a dissipative driven quantum system is often dominated by one particular Floquet state. Depending on the system parameters and the driving frequency, this may be the state with a certain quasienergy [17, 18] or the one with the smallest mean energy [19]. At avoided [19] or exact [18] level crossings of the Floquet spectrum, however, the stationary state may turn from an (almost) pure state to a mixed state made up of several Floquet states. Despite these theoretical advances in relating Floquet state dynamics to spectral properties of strongly driven quantum systems, corresponding experimental investigations [20] in semiconductor systems are scarce.

Cavity quantum electrodynamics [21] allows the study of atom-photon interaction at the single quantum level [22–27]. Recent progress in hybrid circuit quantum electrodynamics (cQED) systems, composed of high quality microwave resonators and semiconductor double quantum dots (DQDs), enables similar explorations in these artificial atoms at the microwave regime. For example, it has been shown that strong electron-photon coupling can be realized in such a cQED system [28–33], and photon-mediated interaction can provide long-distance coupling between qubits [34–37]. An additional benefit of a high quality resonator is that it can also act as a high-sensitivity dispersive photonic probe of the DQD [38, 39], as is widely done for superconducting qubits [40, 41].

In this work, we study the strongly driven dynamics of a two-level system by performing Floquet spectroscopy in a DQD-resonator hybrid system. When we apply a continuous microwave tone onto the DQD, the nonequilibrium population of the eigenstates displays novel features in the cavity-assisted LZSM interference patterns measured by the high-impedance superconducting resonator. In particular, when the hybrid system is driven near half of the resonator frequency, there arise in the interference fringes crescent-shaped holes, where reflectance peaks acquire troughs in analogy to optical hole-burning [42]. Applying the theory for dispersive readout of driven systems [16], we reveal that this phenomenon is caused by a redistribution of the Floquet state population at avoided quasienergy crossings where the system experiences a double resonance, and can be controlled via the driving parameters.

Our device consists of a semiconductor DQD and a 1/4 wavelength superconducting quantum interference device (SQUID) array resonator with a high impedance of $Z_\mathrm{r} \approx 1\,\mathrm{k}\Omega$, as illustrated in Fig. 1(a). A few electrons are trapped in the DQD defined electrically within a GaAs/AlGaAs heterostructure. The electron occupation (m, n) of the DQD is controlled by gate voltages V_L and V_R, as depicted in the charge stability diagram in Fig. 1(b). In the parameter range considered, the DQD dynamics is restricted to the charge states with one ex-

* These authors contributed equally to this work.
† sigmund.kohler@icmm.csic.es
‡ gcao@ustc.edu.cn
§ gpguo@ustc.edu.cn

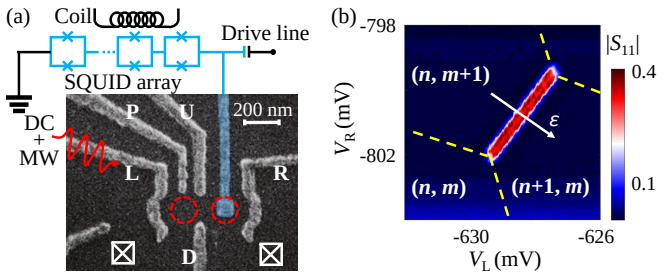

FIG. 1. (a) Scanning electron micrograph of the device. Two quantum dots indicated by dotted circles are defined by metallic top gates. The right plunger gate is connected to the SQUID array resonator. The qubit is driven by continuous microwave tone via the gate L. (b) Charge stability diagram of the DQD measured by the resonator.

cess electron in the left or right QD, denoted by $|L\rangle$ and $|R\rangle$, respectively. Within this basis, the DQD Hamiltonian can be written as $H_0 = \varepsilon\sigma_z/2 + t_c\sigma_x$, where ε is the detuning between $|L\rangle$ and $|R\rangle$ controlled by V_L, t_c is the interdot tunnel coupling, while σ_z and σ_x are Pauli matrices. Diagonalizing H_0, we obtain the energy splitting of a free qubit, $\Delta E = \sqrt{\varepsilon^2 + (2t_c)^2}$.

The DQD is connected via the right plunger gate [blue in Fig. 1(a)] to a high-impedance SQUID array resonator with a tunable resonance frequency ν_r. Unless specified otherwise, $\nu_r = 6.51\,\mathrm{GHz}$. The internal loss rate, external coupling rate and total linewidth of the resonator are $(\kappa_i, \kappa_e, \kappa)/2\pi = (31.0, 34.2, 65.2)\mathrm{MHz}$ [43]. Taking advantage of the high impedance of the resonator, our DQD-resonator system achieves a coupling strength $g_c/2\pi \approx 70\,\mathrm{MHz}$ [37] at resonance $\Delta E/h = \nu_r$ for $2t_c/h = 6.2\,\mathrm{GHz}$, where h is the Planck constant. The coupling strength is larger than both qubit decoherence rate $\gamma/2\pi \approx 50\,\mathrm{MHz}$ and photon loss rate $\kappa/2\pi \approx 65.2\,\mathrm{MHz}$, indicating that the cQED system operates in the strong coupling limit [28–30], which enables a photonic probe with better resolution than conventional $50\,\Omega$ resonators.

We apply a continuous microwave modulation to the left barrier gate L, such that the interdot detuning acquires a time dependence $\varepsilon \to \varepsilon + A\cos(2\pi f_d t)$, where A is the microwave amplitude, $f_d = 1/T$ and T is the period of the driving. The system can thus be described by Floquet theory [44], see Appendix B, which states that the Schrödinger equation has solutions of the form $e^{-2\pi i\mu_\alpha t/h}|\phi_\alpha(t)\rangle$, $\alpha = 0, 1$, where $|\phi_\alpha(t)\rangle$ are the Floquet states satisfying $|\phi_\alpha(t+T)\rangle = |\phi_\alpha(t)\rangle$. The phase factor is governed by the quasienergy μ_α, which is distinct from the mean energy defined as the time-average of the energy expectation value, $E_\alpha \equiv \frac{1}{T}\int_0^T \mathrm{d}t\langle\phi_\alpha(t)|H(t)|\phi_\alpha(t)\rangle$. The Floquet states can be Fourier decomposed into components separated by the energy quantum of the driving field, hf_d, as sketched in Fig. 2(a). The quasienergy splitting $\mu \equiv \mu_1 - \mu_0$ determines the relative phase $2\pi\mu T/h$ between two Floquet states acquired during one driving period. When this phase is close to a multiple of 2π, i.e., when $\mu/h \approx kf_d$ with an integer k, the two Floquet states will interfere constructively, so that both become significantly populated [1]. Consequently, LZSM patterns appear in conductance or electron occupation when such a driven DQD is probed via transport or charge sensing [5, 7, 10].

The driven dynamics of our DQD is probed by the connected microwave resonator [40]. Specifically, we send in a microwave tone via the resonator and measure its reflection. We choose the probe microwave to be at resonance with the resonator, so that the coupling between the DQD and the resonator causes a dispersive frequency shift $\nu_r \to \nu_r + (g_c^2/2\pi)\chi^{(0)}(\nu_r)$ [16], which modifies the reflection. The central quantity here is the phase-averaged susceptibility $\chi^{(0)}$ of the DQD dipole operator [16],

$$\chi^{(0)}(\nu) = (p_0 - p_1)\sum_k \frac{|Z_{10,k}|^2}{2\pi\nu - 2\pi\mu/h + 2\pi k f_d + i\gamma/2}, \tag{1}$$

where $Z_{10,k}$ is the kth Fourier component of the transition matrix element $\langle\phi_0(t)|\sigma_z|\phi_1(t)\rangle$, and p_α is the occupation probability of the Floquet state $|\phi_\alpha\rangle$ in the stationary limit. The p_α are obtained as the well-defined stationary solution of a Bloch-Redfield master equation which allows a realistic description of the weakly dissipative qubit. Details and full expressions can be found in Appendix B.

According to Eq. (1), $\chi^{(0)}(\nu)$ and hence the cavity reflection assume an appreciable size when two conditions are fulfilled. First, with the probe frequency set at the resonator frequency $\nu = \nu_r$, the denominator yields the resonance condition $\mu/h = \nu_r + k' f_d$ for some integer k'. It resembles the resonance condition for the population, but contains an additional cavity photon. The modified fringes observed in the reflection can thus be interpreted as cavity-assisted LZSM interference with one state dressed by a cavity photon [11, 16, 45, 46]. Second, one Floquet state must be predominantly populated such that $|p_0 - p_1| \approx 1$. Figure 2(b) shows such Floquet spectroscopy measured by the reflectance of the resonator $|S_{11}|$ as a function of interdot detuning ε and drive power $P \propto A^2$ for $f_d = 2.5\,\mathrm{GHz}$ and $2t_c/h \approx 6.2\,\mathrm{GHz}$. As expected, the LZSM pattern is similar to the one reported in Ref. [45].

An interesting and qualitatively new situation arises when the resonance conditions for both the transition between Floquet states and the cavity-assisted transition coincide, i.e., when the system reaches the double resonance

$$kf_d = \mu/h = \nu_r + k' f_d\,. \tag{2}$$

This implies that the drive frequency obeys $f_d = \nu_r/2, \nu_r/3, \ldots$ ($f_d = \nu_r$ is discarded because it would directly affect the cavity and pollute the measurement).

Figure 2(c) shows the LZSM pattern for the "one-half resonance" $f_d = 3.3\,\mathrm{GHz} \approx \nu_r/2$. Compared to the cavity-assisted LZSM pattern in Fig. 2(b), every fringe splits up and acquires a crescent-shaped hole, where the

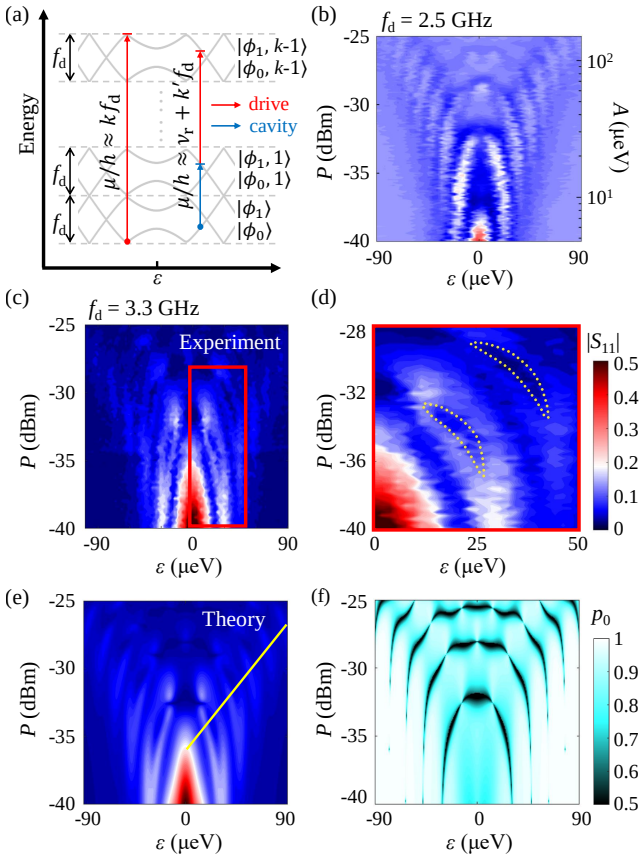

FIG. 2. (a) Schematic energy level diagram explained by Floquet theory. The quasienergy spectrum of the Floquet states has a Brillouin zone structure, which is defined by multiples of the energy quantum of the driving field, hf_d. The state transfer between the two Floquet states, $|\phi_0\rangle$ and $|\phi_1, k\rangle$, can be realized with the population resonance condition (red arrow) or cavity-assisted LZSM resonance condition (blue arrow plus red arrow). (b)–(c) LZSM interference for different drive frequencies f_d. Resonator reflectance $|S_{11}|$ measured as a function of detuning ε and drive power P for $f_d = 2.5\,\mathrm{GHz}$ (b), 3.3 GHz (c), and $2t_c/h \approx 6.2\,\mathrm{GHz}$. (d) A zoom-in view of panel (c). The crescent-like holes are outlined using yellow dotted lines. (e) Simulated result for the parameters used in panel (c), where $P = -29\,\mathrm{dBm}$ corresponds to $A = 60\,\mu\mathrm{eV}$. To consider an inhomogeneous broadening of the LZSM interference pattern induced by the slow fluctuations of the detuning ε [6, 7, 11], all theoretical plots are convoluted with a Gaussian of width 2.5 μeV. The yellow line marks the parameters used in Fig. 3. (f) Calculated mean population of the Floquet state $|\phi_0\rangle$.

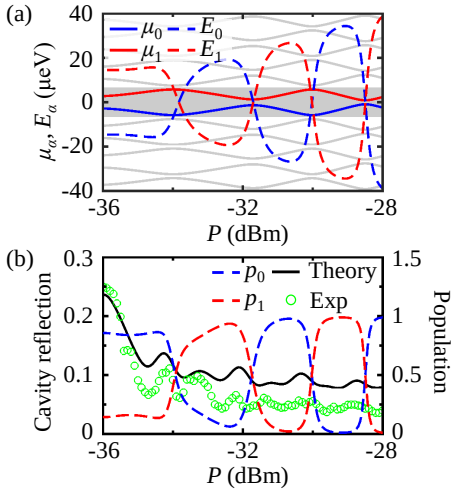

FIG. 3. (a) Floquet spectrum (solid) in the first Brillouin zone (shaded area) and corresponding mean energies (dashed). Gray lines mark the sidebands of the quasienergies. The microwave power and the detuning are both varied along the line in Fig. 2(e). (b) Corresponding populations in the stationary state (dashed) together with the measured (circles) and the simulated (solid) cavity response.

reflection is strongly suppressed. The emergence of these "crescents" can be attributed to the strong driving effect on the Floquet state occupation that modifies the cavity-assisted LZSM interference patterns.

The impact of Floquet state occupation dynamics can be seen in the expression of the susceptibility (1). While the denominators give the cavity-assisted LZSM resonance conditions, the occupation probability p_α also plays an important role. When the resonance condition for the transition between the Floquet states, $\mu/h = kf_d$, is fulfilled, the constructive interference between the Floquet states leads to a significant population of both states, such that $p_1 \approx p_0 = 1/2$ and $p_0 - p_1 \approx 0$. Consequently, $\chi^{(0)}$ is strongly suppressed, and the cavity signal diminishes. A numerical simulation based on Eq. (1) is shown in Fig. 2(e), which is in good agreement with the experiment. The expected population of the Floquet state with smaller quasienergy in Fig. 2(f), confirms that the crescents emerge when the population of this state is significantly reduced.

The analysis above provides an intuitive and qualitative picture for the emergence of the crescents in the cavity-assisted LZSM patterns, and points to the importance of the Floquet state spectrum and population. We thus examine them more closely, and calculate the mean energies and populations of the Floquet states. The solid lines in Fig. 3(a) show the quasienergies $\mu_{0,1}$ and their replica for parameters marked by the line in Fig. 2(e). Most significant are the avoided quasienergy crossings located at the center and border of the Brillouin zone. Since the crossings are avoided, the resonance condition for the population, $\mu = khf_d$, will only be fulfilled approximately. At the avoided quasienergy crossings, the mean energies generically cross exactly, see Appendix B.

The key to the cavity response, however, is not whether $\mu = khf_d$ can be satisfied exactly, but how the populations of the Floquet states behave. As shown in Fig. 3(b), the Floquet state with lower mean energy is populated predominantly. In this case the prefactor of the susceptibility (1) is of the order unity. However, at the avoided quasienergy crossings, the populations in both Floquet states are equal, $p_0 = p_1 = 1/2$. Consequently, the DQD

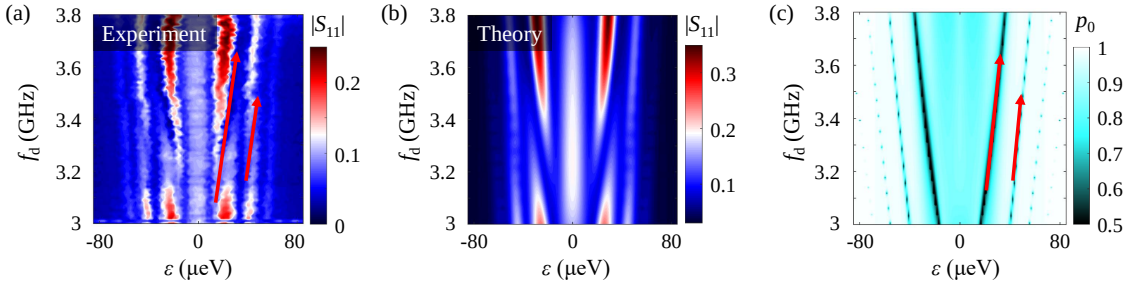

FIG. 4. (a) Resonator reflectance $|S_{11}|$ as a function of detuning ε and drive frequency f_d for power $P = -36\,\mathrm{dBm}$ and $2t/h = 6.2\,\mathrm{GHz}$. The evolution of the crescents is indicated by red arrows. (b) Numerical simulation for the parameters used in panel (a). (c) Corresponding mean population of the Floquet state $|\phi_0\rangle$.

susceptibility vanishes and the simulated cavity reflection assumes its minimum. In comparison, the corresponding experimental result is plotted with circles in Fig. 3(b). It shows good agreement for the positions of the minima. The magnitude of the reflection, including the visibility of the fringes, is predicted fairly well, too. For drive power beyond the second crossing, the agreement becomes more qualitative because the heating effect caused by the large power deteriorates the system coherence. Nevertheless, the agreement between experiment and simulation clearly shows that dispersive readout by a cavity can be employed to probe changes of the stationary Floquet state population and quasienergy crossings.

With cavity frequency ν_r fixed, the double resonance conditions can be satisfied when sweeping both the drive frequency f_d and the qubit detuning ε. As discussed above, we expect a peak in the cavity reflection for $\mu/h = \nu_r + k' f_d$, while a valley emerges for $\mu/h = k f_d$. With $\mu/h = \nu_r + k' f_d = k f_d$ $(k \neq k')$, we expect that as a function of f_d, the peaks and valleys in the cavity reflection in the spectroscopy have different inclinations and cross each other.

Figure 4(a) depicts this feature of the measured reflection as a function of ε and f_d in the vicinity of the one-half resonance $\nu_r/2$ at a fixed driving power. As expected, upon increasing f_d, the gaps (signifying suppression of reflection) in the cavity fringes evolve outwards and intersect the interference stripes when $f_d = \nu_r/2$. A selection of the corresponding LZSM patterns is shown in Appendix A. The simulated measurement in Fig. 4(b) is in good agreement with the experiment. The reduced population of the Floquet state $|\phi_0\rangle$ can be identified as the origin of the collapsing cavity signal. We also computed the expected population of the Floquet state, as shown in Fig. 4(c). Indeed, along the gaps in the interference strips, p_0 is reduced to a value considerably below unity. In short, Fig. 4 not only reconfirms the interplay between the two resonances, but also demonstrates how we can influence and electrically control the dynamics of Floquet states.

With our high-impedance superconducting resonator we were able to measure a crescent-like pattern near the one-half resonance $f_d = \nu_r/2$. Theoretically, one would expect to find a similar structure for $f_d = \nu_r/3, \nu_r/4, \ldots$ However, the LZSM fringes in the populations will be narrow with decreasing drive frequency [1] such that the narrow crescents are blurred by the typical inhomogeneous broadening in GaAs [6, 47]. Nevertheless, we could still observe the characteristic feature of the one-third resonance, which appears as claw-shaped patterns at the end of the interference fringes as shown in Fig. 7 in Appendix A.

In conclusion, we have demonstrated a novel interference pattern in the Floquet spectroscopy of a driven semiconductor DQD probed by a high-impedance resonator. Specifically, when the driving microwave tone is at half of the resonator frequency, crescent-shaped holes/depressions appear in the LZSM interference peaks of the cavity reflection. The physical origin can be explained by the reduced cavity response due to the population redistribution of Floquet states. A systematic investigation revealed that the resonance condition for the population is approximately fulfilled at avoided quasienergy crossings at which the stationary state of the DQD turns from an almost pure state into a mixture. Therefore the emergence of the crescents can be considered as an experimental signature of the nature of the stationary state of a strongly driven two-level system. The LZSM patterns emerging from double resonance are not particular to semiconductor-resonator hybrid systems, but should be generic for all cQED systems. They may be used to gain further insight into Floquet state dynamics in the presence of strong driving.

ACKNOWLEDGMENTS

This work was supported by the National Key Research and Development Program of China (Grant No. 2016YFA0301700), the National Natural Science Foundation of China (Grants No. 61922074, 11674300, 61674132, 11625419 and 11804327), the Strategic Priority Research Program of the CAS (Grant No. XDB24030601), the Anhui initiative in Quantum Information Technologies (Grant No. AHY080000), the Spanish Ministry of Science, Innovation, and Universities (Grant No. MAT2017-

86717-P) and by the CSIC Research Platform on Quantum Technologies PTI-001. H.-W. J. and X. H. acknowledge financial supported by U.S. ARO through Grants No. W911NF1410346 and No. W911NF1710257, respectively. This work was partially carried out at the University of Science and Technology of China Center for Micro and Nanoscale Research and Fabrication.

Appendix A: Additional data

1. LZSM patterns for different drive frequencies

Here we illustrate how the crossing of the bright and the dark stripe [see Fig. 4 of the main text] manifests itself in the LZSM pattern. To this end, we slightly vary f_d around the half-resonance $\nu_\mathrm{r}/2$. The resulting measured patterns are shown in Fig. 5. With increasing drive frequency f_d, the crescent-shaped holes in the fringes move outwards, which correspond to a shift along the red arrows in Fig. 4(a).

2. Tuning the resonator frequency

Taking advantage of the tunability of the SQUID array resonator, we are able to vary also the resonance frequency ν_d by the current I_coil of a cm-sized coil mounted on the sample holder from 6.5 GHz to below 5.2 GHz as shown in Fig. 6(a). Tuning the resonance frequency ν_r from 6.51 GHz to 6.07 GHz while keeping the drive frequency at $f_\mathrm{d} = 3.3$ GHz, the crescents in Fig. 6(d) vanish once the condition for double resonance, $\nu_\mathrm{r} = nf_\mathrm{d}$ with $n \geq 2$, is sufficiently violated. In contrast, when we decrease f_d to 2.9 GHz which is close to $\nu_\mathrm{r}/2$ (for f_d a value below one-half resonance 3 GHz may result from the shift of the resonance frequency due to the fluctuation of the magnetic environment), crescents arise again in Fig. 6(c). Thus, we have tested our conjecture for the interplay of cavity reflection and Floquet state population by independently varying all relevant frequencies.

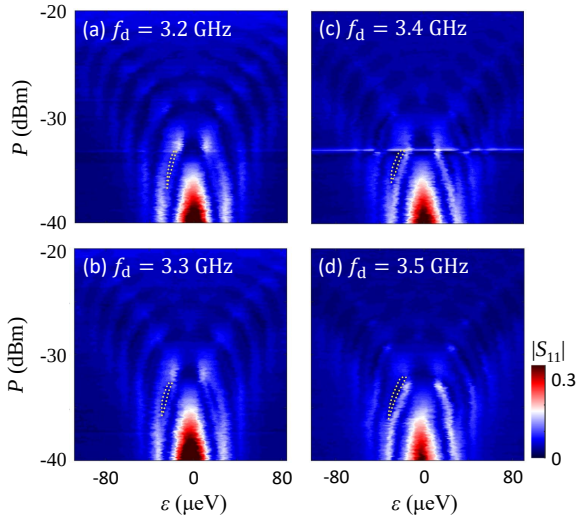

FIG. 5. LZSM interference patterns for various drive frequencies f_d near the half-resonance $\nu_\mathrm{r}/2$ ranging from 3.2 GHz to 3.5 GHz. The crescents are outlined by yellow doted lines.

3. Crescents of higher order

In the experiment, we have observed crescents only for the one-half resonance $f_\mathrm{d} \approx \nu_\mathrm{r}/2$. For resonances of higher order, i.e., for $f_\mathrm{d} \approx \nu_\mathrm{r}/k$ with $k > 2$, similar patterns are expected to be observed. However, the LZSM fringes in the populations will diminish with decreasing drive frequency [1] such that their size eventually drops below the experimental resolution.

We show in Fig. 7(a) the theoretical prediction for the cavity reflection near the one-third resonance, which exhibits very narrow crescents. However, to predict the result of a realistic measurement, we have to take into account that the level detuning ε is slowly fluctuating. This causes an inhomogeneous broadening of the order of some μeV [7, 47] which can be captured by convolving the theory data with a Gaussian of corresponding width. Figure 7(b) depicts the resulting prediction for a measurement, where we have assumed a broadening of 2.5 μeV. This blurs the LZSM pattern so much that the narrow crescents practically disappear. Nevertheless, we could still find the characteristic feature of the one-third

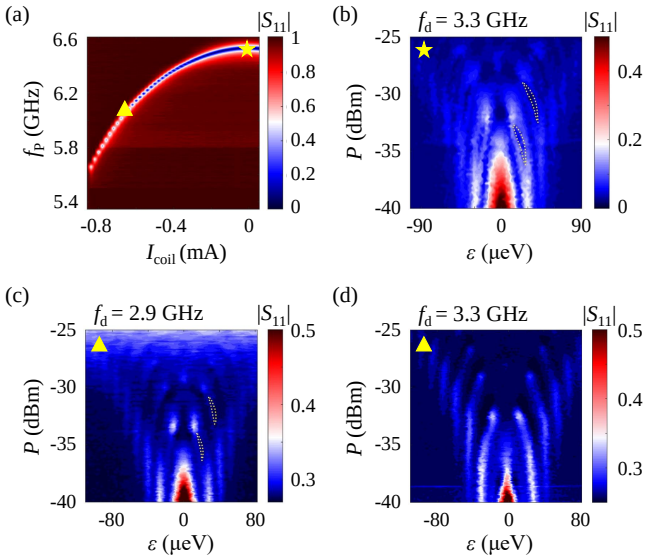

FIG. 6. (a) Reflectance spectrum $|S_{11}|$ as a function of probe frequency ν_p and current I_coil through the coil. Resonance frequency ν_r is tuned from 6.51 GHz to 6.07 GHz indicated by a star and a triangle, respectively. (b–d) Interference patterns for different ν_r in (a) and different f_d.

resonance, which appears as claw-shaped patterns at the end of the interference fringes. Figure 7(d) demonstrates these claw-shaped patterns measured in the experiment.

Appendix B: Theoretical background and methods

In the following, we briefly review the theoretical tools and concepts used in the main text.

1. Floquet theory

The Schrödinger equation of a T-periodically driven quantum system possesses a complete set of solutions of the form [44]

$$|\psi_\alpha(t)\rangle = e^{-i\mu_\alpha t/\hbar}|\phi_\alpha(t)\rangle, \tag{B1}$$

where the Floquet states $|\phi_\alpha(t)\rangle$ obey the periodicity of the driving, while the quasienergies μ_α determine the phase acquired by $|\psi_\alpha(t)\rangle$ during one driving period. Both the quasienergies and the Floquet states can be obtained by solving the Floquet eigenvalue equation

$$\mathcal{H}(t)|\phi(t)\rangle \equiv \Big(H(t) - i\hbar\frac{d}{dt}\Big)|\phi(t)\rangle = \mu|\phi(t)\rangle. \tag{B2}$$

The quasienergy spectrum has a Brillouin zone structure, which means that they are defined only up to multiples of the energy quantum of the driving field, $\hbar\Omega$, where $\Omega = 2\pi/T$ is the angular frequency of the driving. As the quasienergies follow from an eigenvalue equation, they exhibit level repulsion, i.e., in the absence of symmetries they generically form avoided crossings. At such avoided crossings the participating states interchange their physical properties, in particular their mean energies

$$E_\alpha = \frac{1}{T}\int_0^T dt\,\langle\psi_\alpha(t)|H(t)|\psi_\alpha(t)\rangle. \tag{B3}$$

This implies that at avoided quasienergy crossings, the corresponding mean energies cross exactly.

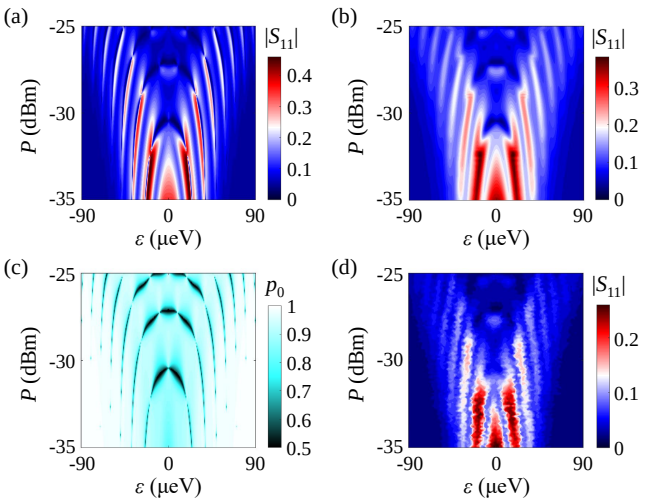

FIG. 7. (a) Theoretical prediction for the cavity response for the one-third resonance with driving frequency $f_\mathrm{d} = 2.27\,\mathrm{GHz} \approx \nu_\mathrm{r}/3$ at which the drive power $-29\,\mathrm{dBm}$ corresponds to $A = 45\,\mu\mathrm{eV}$. (b) The same data, but after considering for the detuning ε an inhomogeneous broadening of $2.5\,\mu\mathrm{eV}$. (c) Corresponding mean population of the Floquet state $|\phi_0\rangle$. (d) Experimental data for the resonator reflectance $|S_{11}|$ with $f_\mathrm{d} = 2.27\,\mathrm{GHz}$.

2. Floquet spectrum of the two-level system

In the main text, we describe the DQD by the two-level Hamiltonian

$$H(t) = \frac{\Delta}{2}\sigma_x + \frac{\varepsilon + A\cos(\Omega t)}{2}\sigma_z\,, \tag{B4}$$

where Δ is the interdot tunnel coupling, A is the drive amplitude and $\sigma_{x,y,z}$ are Pauli matrices. Let us consider the transformation of the corresponding Floquet Hamiltonian $\mathcal{H} = H(t) - i\hbar\,d/dt$ under the anti-unitary transformation $\theta = i\sigma_y K$, where K causes complex conjugation, i.e., $KzK^{-1} = z^*$. One readily sees that $\theta\mathcal{H}(t)\theta^{-1} = -\mathcal{H}(t)$ (notice that for the present reasoning, we do not invert the time argument of the Hamiltonian), which implies that any solution of the Floquet equation (B2) with eigenvalue μ has a time-reversed partner with eigenvalue $-\mu$. It is therefore convenient to choose the Brillouin zone symmetrically around zero, $-\hbar\Omega/2 < \mu_\alpha \le \hbar\Omega/2$, which for the two-level system ensures the relation $\mu_0 + \mu_1 = 0$.

It is now tempting to conclude that (exact) quasienergy crossings can occur only when $\mu_0 = \mu_1 = 0$. This however, would ignore crossings with equivalent states from other Brillouin zones with quasienergies shifted by multiples of $\hbar\Omega$. Taking them into account yields for the crossings the weaker condition $\mu_0 + k\hbar\Omega = \mu_1$, where k may be any integer, such that $\mu_0 = k\hbar\Omega/2$. This means that for the Hamiltonian (B4), quasienergies may cross only at the border or in the middle of the Brillouin zone. In the absence of symmetries, the crossings are generally avoided, but nevertheless are found under the same condition, see Fig. 3(a).

3. Stationary state of a driven system

In quantum mechanics, dissipation can be modeled by coupling the system to a heat bath. For weak dissipation, one may eliminate the bath by second order perturbation theory to obtain a Markovian master equation for the reduced density operator. For a driven system, Floquet states form a suitable basis for the numerical treatment of such master equations, because then the driving is already included by the choice of the basis [48]. Finally,

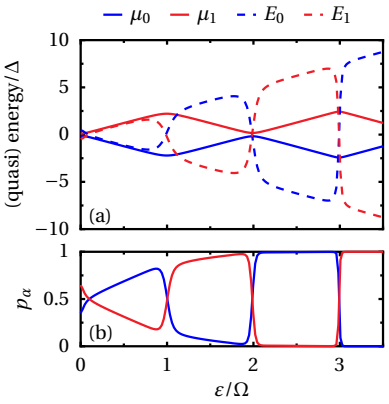

FIG. 8. (a) Quasienergies (solid lines) and mean energies (dashed) for the driven two-level system as function of the detuning for driving frequency $\Omega = 5\Delta$ and amplitude $A = 2\Omega$ at zero temperature in the weak coupling limit. The bath couples to the system operator σ_x. (b) Populations of the corresponding Floquet states in the stationary limit.

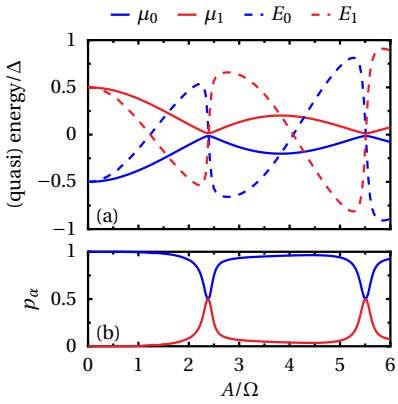

FIG. 9. The same as Fig. 8 for detuning $\varepsilon = 0.03\Delta$ as function of the driving amplitude for a bath coupled via σ_z, which far from the quasienergy crossings leads to a Floquet-Gibbs state.

one obtains for the populations p_α of the Floquet states a rate equation of the form

$$\dot{p}_\alpha = \sum_\beta (w_{\alpha\leftarrow\beta} p_\beta - w_{\beta\leftarrow\alpha} p_\alpha). \tag{B5}$$

The transition rates $w_{\alpha\leftarrow\beta}$ are given by golden-rule like expressions for the transition matrix elements of the operator that couple the system to the bath. In the numerical calculations of the main text, this coupling is established via the qubit operator σ_x. This choice leads to the observed generic LZSM pattern [49] and fits the observation rather well.

Generally, this master equation possesses a unique stationary solution with $\dot{p}_\alpha = 0$ for all α, despite that it does not fulfill a detailed balance condition. The latter makes it virtually impossible to find a generic formal solution for the stationary state. Nevertheless, in a few cases this is possible. Here we sketch two typical limits and apply the ideas to the driven two-level system described by the Hamiltonian (B4).

For small or intermediate frequencies, a natural guess is that the system eventually resides in the Floquet state with the smallest mean energy, possibly with a small admixture of other Floquet states. This was indeed found for systems with mixed chaotic/regular phase space with some exception close to avoided crossings [19]. For the present case of a two-level system, the spectra and the populations are shown in Fig. 8. This confirms that far from the crossings, the state with smaller mean energy is predominantly occupied. At the center of the crossing, however, both states have equal mean energy and, consequently, we observe a mixture of both Floquet states, where each one is occupied with probability $p_0 \approx p_1 \approx 1/2$.

For high-frequency driving, the system may be mapped approximately to a time-independent Hamiltonian [50, 51]. If in addition, the system-bath coupling commutes with the driving, one often finds a Floquet-Gibbs state, i.e., a statistical mixture that resembles a Gibbs states but with the energies replaced by quasienergies [17, 18], provided that the Brillouin zone is chosen such that it covers the spectrum of the undriven system. For the two-level system, this was found for zero detuning [18]. For small detuning this is still valid, as can be appreciated in Fig. 9. In panel (b), we indeed see that, in contrast to Fig. 8(b), the populations are governed by the quasienergies.

These situations emphasize the role of avoided quasienergy crossings for the long-time solution of a driven dissipative quantum system. The characteristic feature is that far from the crossings, one Floquet state dominates, while at the crossings, both states are equally populated. In our experiment, these equal populations are responsible for the emergence of crescents in the LZSM patterns.

4. AC-driving and dispersive readout

A Floquet theory for the response of a microwave cavity coupled to a periodically driven double quantum dot (DQD) has been derived in Ref. [16]. Its cornerstones are summarized in the following. The central idea of dispersive readout is that a resonantly driven cavity acts via a coupling $H_{\rm coupl} = g_{\rm c} Z(a + a^\dagger)$ with some system operator Z and the creation and annihilation operators $a^\dagger$ and a of a cavity photon on the DQD (or any other quantum system). In turn the DQD acts back to the cavity, which leads to a frequency shift of the cavity that provides information on the DQD state. Within linear-response theory, this backaction is captured by the susceptibility $\chi(t,t') = -i\langle[Z(t), Z(t')]\rangle\theta(t-t')$ with θ the Heaviside step function and $Z = \sigma_z$ the operator that couples the DQD to the cavity. If the DQD experiences an additional external driving, the susceptibility depends

explicitly on both times. In the case of periodic driving, after a transient stage, $\chi(t,t') = \chi(t+T,t'+T)$, which implies that $\chi(t,t-\tau)$ with $\tau = t-t'$ is T-periodic in t.

The susceptibility χ allows one to calculate via input-output theory [40, 52] the reflection of our one-sided cavity to read

$$S_{11} = \frac{a_{\rm out}}{a_{\rm in}} = 1 + \frac{i\kappa_{\rm i}}{\omega_c - \omega + g_c^2\chi^{(0)}(\omega) - i\kappa/2}\,, \quad \text{(B6)}$$

where $\kappa_{\rm i,e}$ are the internal and external loss rates of the cavity, while the total loss $\kappa = \kappa_{\rm i} + \kappa_{\rm e}$.

The impact of the DQD is contained in the $k = 0$ component of the Fourier transformed susceptibility

$$\chi^{(k)}(\omega) = \int_0^\infty \left[\frac{1}{T}\int_0^T e^{ik\Omega t + i\omega t}\chi(t,t-\tau)dt\right]d\tau, \quad \text{(B7)}$$

where for $k = 0$ the t-integration corresponds to the average over one driving period which is equivalent to averaging over the phase of the driving. When the DQD is described by a density operator $\rho_\infty = \sum_\alpha p_\alpha |\phi_\alpha(t)\rangle\langle\phi_\alpha(t)|$ with probabilities p_α computed as described above, one obtains for the susceptibility after some algebra the expression [16]

$$\chi^{(0)}(\omega) = \sum_{\alpha,\beta,k} \frac{(p_\alpha - p_\beta)|Z_{\alpha\beta,k}|^2}{\omega + \mu_\alpha - \mu_\beta - k\Omega + i\gamma_{\alpha\beta}/2}. \quad \text{(B8)}$$

Here, $Z_{\alpha\beta,k}$ denotes the kth Fourier component of the T-periodic transition matrix element $Z_{\alpha\beta}(t) = \langle\phi_\alpha(t)|Z|\phi_\beta(t)\rangle$, while the dephasing rates $\gamma_{\alpha\beta}$ have been introduced phenomenologically.

[1] S. N. Shevchenko, S. Ashhab, and F. Nori, Landau-Zener-Stückelberg interferometry, Phys. Rep. **492**, 1 (2010).

[2] M. P. Silveri, J. A. Tuorila, E. V. Thuneberg, and G. S. Paraoanu, Quantum systems under frequency modulation, Rep. Prog. Phys. **80**, 056002 (2017).

[3] W. D. Oliver, Y. Yu, J. C. Lee, K. K. Berggren, L. S. Levitov, and T. P. Orlando, Mach-Zehnder interferometry in a strongly driven superconducting qubit, Science **310**, 1653 (2005).

[4] M. Sillanpää, T. Lehtinen, A. Paila, Y. Makhlin, and P. Hakonen, Continuous-time monitoring of Landau-Zener interference in a Cooper-pair box, Phys. Rev. Lett. **96**, 187002 (2006).

[5] J. Stehlik, Y. Dovzhenko, J. R. Petta, J. R. Johansson, F. Nori, H. Lu, and A. C. Gossard, Landau-Zener-Stuckelberg interferometry of a single electron charge qubit, Phys. Rev. B **86**, 121303(R) (2012).

[6] G. Cao, H.-O. Li, T. Tu, L. Wang, C. Zhou, M. Xiao, G.-C. Guo, H.-W. Jiang, and G.-P. Guo, Ultrafast universal quantum control of a quantum-dot charge qubit using Landau–Zener–Stückelberg interference, Nature Commun. **4**, 1401 (2013).

[7] F. Forster, G. Petersen, S. Manus, P. Hänggi, D. Schuh, W. Wegscheider, S. Kohler, and S. Ludwig, Characterization of qubit dephasing by Landau-Zener-Stückelberg-Majorana interferometry, Phys. Rev. Lett. **112**, 116803 (2014).

[8] M. P. Silveri, K. S. Kumar, J. Tuorila, J. Li, A. Vepsäläinen, E. V. Thuneberg, and G. S. Paraoanu, Stückelberg interference in a superconducting qubit under periodic latching modulation, New J. Phys. **17**, 043058 (2015).

[9] M. F. Gonzalez-Zalba, S. N. Shevchenko, S. Barraud, J. R. Johansson, A. J. Ferguson, F. Nori, and A. C. Betz, Gate-sensing coherent charge oscillations in a silicon field-effect transistor, Nano Letters **16**, 1614 (2016).

[10] A. Bogan, S. Studenikin, M. Korkusinski, L. Gaudreau, P. Zawadzki, A. S. Sachrajda, L. Tracy, J. Reno, and T. Hargett, Landau-Zener-Stückelberg-Majorana interferometry of a single hole, Phys. Rev. Lett. **120**, 207701 (2018).

[11] X. Mi, S. Kohler, and J. R. Petta, Landau-Zener interferometry of valley-orbit states in Si/SiGe double quantum dots, Phys. Rev. B **98**, 161404(R) (2018).

[12] Y. Han, X.-Q. Luo, T.-F. Li, W. Zhang, S.-P. Wang, J. Tsai, F. Nori, and J. You, Time-domain grating with a periodically driven qutrit, Phys. Rev. Applied **11**, 014053 (2019).

[13] P. Y. Wen, O. V. Ivakhnenko, M. A. Nakonechnyi, B. Suri, J.-J. Lin, W.-J. Lin, J. C. Chen, S. N. Shevchenko, F. Nori, and I.-C. Hoi, Landau-Zener-Stückelberg-Majorana interferometry of a superconducting qubit in front of a mirror, Phys. Rev. B **102**, 075448 (2020).

[14] D. M. Berns, M. S. Rudner, S. O. Valenzuela, K. K. Berggren, W. D. Oliver, L. S. Levitov, and T. P. Orlando, Amplitude spectroscopy of a solid-state artificial atom, Nature (London) **455**, 51 (2008).

[15] A. Ferrón, D. Domínguez, and M. J. Sánchez, Dynamic transition in Landau-Zener-Stckelberg interferometry of dissipative systems: The case of the flux qubit, Phys. Rev. B **93**, 064521 (2016).

[16] S. Kohler, Dispersive readout: Universal theory beyond the rotating-wave approximation, Phys. Rev. A **98**, 023849 (2018).

[17] M. Hartmann, D. Poletti, M. Ivanchenko, S. Denisov, and P. Hänggi, Asymptotic Floquet states of open quantum systems: the role of interaction, New J. Phys. **19**, 083011 (2017).

[18] G. Engelhardt, G. Platero, and J. Cao, Discontinuities in driven spin-boson systems due to coherent destruction of tunneling: Breakdown of the Floquet-Gibbs distribution, Phys. Rev. Lett. **123**, 120602 (2019).

[19] S. Kohler, R. Utermann, P. Hänggi, and T. Dittrich, Coherent and incoherent chaotic tunneling near singlet-doublet crossings, Phys. Rev. E **58**, 7219 (1998).

[20] L. Magazzù, P. Forn-Díaz, R. Belyansky, J.-L. Orgiazzi, M. A. Yurtalan, M. R. Otto, A. Lupascu, C. M. Wilson, and M. Grifoni, Probing the strongly driven spin-boson model in a superconducting quantum circuit, Nat. Commun. **9**, 1403 (2018).

[21] S. Haroche and J.-M. Raimond, *Exploring the Quantum: Atoms, Cavities, and Photons* (Oxford University Press, Oxford, 2006).

[22] R. J. Thompson, G. Rempe, and H. J. Kimble, Observation of normal-mode splitting for an atom in an optical cavity, Phys. Rev. Lett. **68**, 1132 (1992).

[23] M. Brune, F. Schmidt-Kaler, A. Maali, J. Dreyer, E. Hagley, J. M. Raimond, and S. Haroche, Quantum Rabi oscillation: A direct test of field quantization in a cavity, Phys. Rev. Lett. **76**, 1800 (1996).

[24] D. I. Schuster, A. P. Sears, E. Ginossar, L. DiCarlo, L. Frunzio, J. J. L. Morton, H. Wu, G. A. D. Briggs, B. B. Buckley, D. D. Awschalom, and R. J. Schoelkopf, High-cooperativity coupling of electron-spin ensembles to superconducting cavities, Phys. Rev. Lett. **105**, 140501 (2010).

[25] Y. Kubo, F. R. Ong, P. Bertet, D. Vion, V. Jacques, A. D. D. Zheng, J.-F. Roch, A. Auffeves, F. Jelezko, J. Wrachtrup, M. F. Barthe, P. Bergonzo, and D. Esteve, Strong coupling of a spin ensemble to a superconducting resonator, Phys. Rev. Lett. **105**, 140502 (2010).

[26] J. D. Teufel, D. Li, M. S. Allman, K. Cicak, A. J. Sirois, J. D. Whittaker, and R. W. Simmonds, Circuit cavity electromechanics in the strong-coupling regime, Nature **471**, 204 (2011).

[27] Y. Tabuchi, S. Ishino, T. Ishikawa, R. Yamazaki, K. Usami, and Y. Nakamura, Hybridizing ferromagnetic magnons and microwave photons in the quantum limit, Phys. Rev. Lett. **113**, 083603 (2014).

[28] A. Stockklauser, P. Scarlino, J. V. Koski, S. Gasparinetti, C. K. Andersen, C. Reichl, W. Wegscheider, T. Ihn, K. Ensslin, and A. Wallraff, Strong coupling cavity QED with gate-defined double quantum dots enabled by a high impedance resonator, Phys. Rev. X **7**, 011030 (2017).

[29] X. Mi, J. V. Cady, D. M. Zajac, P. W. Deelman, and J. R. Petta, Strong coupling of a single electron in silicon to a microwave photon, Science **355**, 156 (2017).

[30] L. E. Bruhat, T. Cubaynes, J. J. Viennot, M. C. Dartiailh, M. M. Desjardins, A. Cottet, and T. Kontos, Circuit QED with a quantum-dot charge qubit dressed by Cooper pairs, Phys. Rev. B **98**, 155313 (2018).

[31] N. Samkharadze, G. Zheng, N. Kalhor, D. Brousse, A. Sammak, U. C. Mendes, A. Blais, G. Scappucci, and L. M. K. Vandersypen, Strong spin-photon coupling in silicon, Science **359**, 1123 (2018).

[32] X. Mi, M. Benito, S. Putz, D. M. Zajac, J. M. Taylor, G. Burkard, and J. R. Petta, A coherent spin-photon interface in silicon, Nature (London) **555**, 599 (2018).

[33] A. J. Landig, J. V. Koski, P. Scarlino, U. C. Mendes, A. Blais, C. Reichl, W. Wegscheider, A. Wallraff, K. Ensslin, and T. Ihn, Coherent spinphoton coupling using a resonant exchange qubit, Nature **560**, 179 (2018).

[34] M. R. Delbecq, L. E. Bruhat, J. J. Viennot, S. Datta, A. Cottet, and T. Kontos, Photon-mediated interaction between distant quantum dot circuits, Nature Comm. **4**, 1400 (2013).

[35] D. van Woerkom, P. Scarlino, J. Ungerer, C. Müller, J. Koski, A. Landig, C. Reichl, W. Wegscheider, T. Ihn, K. Ensslin, and A. Wallraff, Microwave photon-mediated interactions between semiconductor qubits, Phys. Rev. X **8**, 041018 (2018).

[36] F. Borjans, X. G. Croot, X. Mi, M. J. Gullans, and J. R. Petta, Resonant microwave-mediated interactions between distant electron spins, Nature **577**, 195 (2020).

[37] B. Wang, T. Lin, H. Li, S. Gu, M. Chen, G. Guo, H. Jiang, X. Hu, G. Cao, and G. Guo, Correlated spectrum of distant semiconductor qubits coupled by microwave photons, Science Bulletin **66**, 332 (2021).

[38] K. D. Petersson, L. W. McFaul, M. D. Schroer, M. Jung, J. M. Taylor, A. A. Houck, and J. R. Petta, Circuit quantum electrodynamics with a spin qubit, Nature (London) **490**, 380 (2012).

[39] T. Frey, P. J. Leek, M. Beck, A. Blais, T. Ihn, K. Ensslin, and A. Wallraff, Dipole coupling of a double quantum dot to a microwave resonator, Phys. Rev. Lett. **108**, 046807 (2012).

[40] A. Blais, R.-S. Huang, A. Wallraff, S. M. Girvin, and R. J. Schoelkopf, Cavity quantum electrodynamics for superconducting electrical circuits: An architecture for quantum computation, Phys. Rev. A **69**, 062320 (2004).

[41] F. Arute, K. Arya, R. Babbush, D. Bacon, J. C. Bardin, R. Barends, R. Biswas, S. Boixo, F. G. S. L. Brandao, D. A. Buell, B. Burkett, Y. Chen, Z. Chen, B. Chiaro, R. Collins, W. Courtney, A. Dunsworth, E. Farhi, B. Foxen, A. Fowler, C. Gidney, M. Giustina, R. Graff, K. Guerin, S. Habegger, M. P. Harrigan, M. J. Hartmann, A. Ho, M. Hoffmann, T. Huang, T. S. Humble, S. V. Isakov, E. Jeffrey, Z. Jiang, D. Kafri, K. Kechedzhi, J. Kelly, P. V. Klimov, S. Knysh, A. Korotkov, F. Kostritsa, D. Landhuis, M. Lindmark, E. Lucero, D. Lyakh, S. Mandra, J. R. McClean, M. McEwen, A. Megrant, X. Mi, K. Michielsen, M. Mohseni, J. Mutus, O. Naaman, M. Neeley, C. Neill, M. Y. Niu, E. Ostby, A. Petukhov, J. C. Platt, C. Quintana, E. G. Rieffel, P. Roushan, N. C. Rubin, D. Sank, K. J. Satzinger, V. Smelyanskiy, K. J. Sung, M. D. Trevithick, A. Vainsencher, B. Villalonga, T. White, Z. J. Yao, P. Yeh, A. Zalcman, H. Neven, and J. M. Martinis, Quantum supremacy using a programmable superconducting processor, Nature **574**, 505 (2019).

[42] D. F. Walls and G. J. Milburn, *Quantum Optics*, 2nd ed. (Springer, Heidelberg, 1995).

[43] P. J. Petersan and S. M. Anlage, Measurement of resonant frequency and quality factor of microwave resonators: Comparison of methods, J. Appl. Phys. **84**, 3392 (1998).

[44] J. H. Shirley, Solution of the Schrödinger equation with a Hamiltonian periodic in time, Phys. Rev. **138**, B979 (1965).

[45] J. V. Koski, A. J. Landig, A. Pályi, P. Scarlino, C. Reichl, W. Wegscheider, G. Burkard, A. Wallraff, K. Ensslin, and T. Ihn, Floquet spectroscopy of a strongly driven quantum dot charge qubit with a microwave resonator, Phys. Rev. Lett. **121**, 043603 (2018).

[46] S. N. Shevchenko, A. I. Ryzhov, and F. Nori, Low-frequency spectroscopy for quantum multilevel systems, Phys. Rev. B **98**, 195434 (2018).

[47] K. D. Petersson, J. R. Petta, H. Lu, and A. C. Gossard, Quantum coherence in a one-electron semiconductor charge qubit, Phys. Rev. Lett. **105**, 246804 (2010).

[48] S. Kohler, T. Dittrich, and P. Hänggi, Floquet-Markovian description of the parametrically driven, dissipative harmonic quantum oscillator, Phys. Rev. E **55**, 300 (1997).

[49] R. Blattmann, P. Hänggi, and S. Kohler, Qubit interference at avoided crossings: The role of driving shape and bath coupling, Phys. Rev. A **91**, 042109 (2015).

[50] M. Holthaus, Collapse of minibands in far-infrared irradiated superlattices, Phys. Rev. Lett. **69**, 351 (1992).

[51] F. Großmann and P. Hänggi, Localization in a driven two-level dynamics, Europhys. Lett. **18**, 571 (1992).

[52] M. J. Collett and C. W. Gardiner, Squeezing of intracav-

ity and traveling-wave light fields produced in parametric amplification, Phys. Rev. A **30**, 1386 (1984).